PCCP

PAPER

Cite this: *Phys. Chem. Chem. Phys.*, 2018, **20**, 26280

Quantum efficiency of the photo-induced electronic transfer in dye–TiO_2 complexes

Dalma M. Marquez [ab] and Cristián G. Sánchez *[ab]

Received 20th July 2018,
Accepted 2nd October 2018

DOI: 10.1039/c8cp04625e

rsc.li/pccp

We present a method based on a time-dependent self-consistent density functional tight-binding (TD-DFTB) approach, able to predict the quantum efficiency of the photoinjection process in a dye–TiO_2 complex from a fully atomistic picture. We studied the process of charge transfer of three systems with different dyes: catechol (CAT), alizarin (ALZ) and FSD101. Each system was excited with lasers of different energies in the range of 300–2500 nm, studying the efficiency of the induced charge transfer process at the incident energies. We show that the perturbation can produce either hole transfer or electron transfer from the dye to the nanoparticle, therefore affecting the efficiency of the charge transfer in the solar cell when illuminated by broadband radiation.

1 Introduction

Dye-sensitized solar cells (DSSCs) are photovoltaic devices that convert solar energy into electric current. Since the first cell presented in 1991 by O'Regan and Gratzel[1] (Gratzel cell), DSSCs have become a low-cost technology and easy to manufacture alternative to conventional solar cells,[2,3] with an efficiency that has been improving in recent years.

The conventional DSSC or n-type DSSC (Fig. 1, on the left) is composed of a dye anchored to a nano-crystalline n-type semiconductor with a wide band gap like TiO_2.[3] The working mechanism of these cells involves the photo-excitation of the dye, triggering an electron transfer from the LUMO of the molecule to the conduction band (CB) of the nanoparticle (NP), followed by regeneration of the oxidized dye by a redox couple (*e.g.*, I^-/I_3^-) in solution and finally the migration of charges that are collected by a conducting electrode to complete the circuit.[4,5]

While n-type DSSCs are a highly researched area, in recent years, there has been increasing interest in the investigation of p-type DSSCs (Fig. 1, on the right). This technology converts the solar energy through a process of electrochemical reduction induced by light absorption and involves hole injection into the valence band of a p-type semiconductor generating the reduction of the dye. Then, the dye can be regenerated by the redox couple if the rate of charge recombination process between the reduced dye and the hole in the valence band is slow.[6–8]

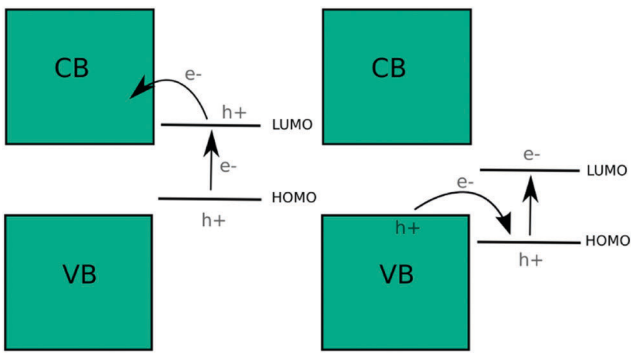

Fig. 1 Left: n-Type sensitization; right: p-type sensitization.

For a DSSC to be successful, all components must be chosen properly: the photoelectrode material, the dye/sensitizer and the redox couple. In n-type DSSCs, anatase phase titanium dioxide (TiO_2) is generally used as a sensitizer, coated over a transparent conducting substrate (TCO) as the photoanode. The main reasons for its use are its many advantages over other semiconductors such as easy synthesis, stability, non-toxicity, low cost and also its larger band-gap compared to the other crystalline forms of TiO_2 (3.2 *vs.* 3.0 eV for rutile).[9]

Nevertheless, in p-type DSSCs, other materials like NiO,[6,10,11] $AgCrO_2$,[12] CuO,[13,14] CuSCN,[15,16] Cu_2O[17] and $CuAlO_2$[18] are commonly utilized to prepare photocathodes. In particular, NiO has been widely used in p-type DSSCs due to its stability, wide band gap (3.6–4.0 eV) and because the potential value of its valence band is suitable for the electron transfer process from the semiconductor to the dye to occur (0.54 V *vs.* NHE at pH 7.30).[6]

The dye, in both kinds of DSSCs, must have certain features for efficient performance, essentially a broad and strong absorption in the visible and near-red spectrum, chemical stability and

[a] *Universidad Nacional de Córdoba, Facultad de Ciencias Químicas, Departamento de Química Teórica y Computacional, Ciudad Universitaria, X5000HUA, Córdoba, Argentina*

[b] *Instituto de Investigaciones Fisicoquímicas de Córdoba, Consejo Nacional de Investigaciones Científicas y Técnicas (INFIQC – CONICET), Ciudad Universitaria, X5000HUA, Córdoba, Argentina. E-mail: cgsanchez@fcq.unc.edu.ar*

appropriate redox potentials of the HOMO and LUMO states for the charge injection and recombination process to be successful.[19] Novel dyes have been studied to increase cell efficiency; for n-type DSSCs, sensitizers such as triphenylamine,[20–22] heterocyclic azo,[23] indoline,[24] triarylamine,[25] carbazole,[21,26] dithienylpyrazine,[27] coumarin,[28–30] porphyrins[31–33] and quinoline[34]-based dyes while for p-type DSSCs, coumarin,[35–38] porphyrin,[39,40] tryarilamine,[41] perylenediimide,[42,43] isoindigo,[44] squaraine,[45] arylamine[46] and carbazole[47,48]-based dyes have been utilized.

In previuos works, our group demonstrated n-type and p-type sensitization of anatase TiO_2[49,50] and $Ti_{17}O_{24}(OPri)_{20}$ nanoparticles,[51] respectively, by several adsorbates, obtaining a good correlation with experimental data. Further elaborating on the basis of our earlier experience, in this work, we show how efficient the transfer process is in dye–semiconductor systems when they are illuminated with broadband radiation. For that, we studied three dye–TiO_2 systems using dyes whose conjugate structures make them good sensitizers for DSSCs, alizarine (ALZ)[49] and catechol (CAT),[50] and on the other hand, FSD101,[20] since very good efficiencies have been obtained with dyes having triple bonds in their structure.[32,33,52] In addition to calculating the spectra of the dye–TiO_2 systems and reporting a detailed analysis of the photoinduced charge transfer process between different dyes and TiO_2 illuminated with a perturbation tuned with the energy of the maximum of the spectrum, we study the electron dynamics of the system when illuminating with all the wavelengths of the solar spectrum at sea level, and with these results, we calculate the quantum efficiency of the photo-induced dye–nanoparticle charge transfer. All simulations presented here are based on a real-time time-dependent density functional tight-binding (RT-TD-DFTB) model, which describes the system under non-equilibrium conditions.

2 Computational method

The electronic structure of the ground state of all systems was described by the SCC-DFTB method,[53] which is based on the second-order expansion of the total energy of KS with respect to electronic density fluctuations. The implementation of the SCC-DFTB method used in this work is the dftb$^+$ package.[54] The dftb$^+$ is used to obtain the Hamiltonian, the overlap matrix and the mono-electronic density matrix of the ground state. We have utilized the mio-0-1[53] and tiorg-1-1[55] parameter sets for all the calculations shown.

The electronic dynamics were simulated through the TD-SCC-DFTB method, which is an extension of the SCC-DFTB method to the time domain, based on the evolution of the reduced single-particle ground state density matrix (obtained previously with the dftb$^+$ package) in the presence of a time-dependent external perturbation. Integrating the Liouville-von Neumann equation of motion on a non-orthogonal basis yields the evolution of the density matrix:

$$\frac{\partial\hat{\rho}}{\partial t} = \frac{1}{i\hbar}\left(S^{-1}\hat{H}[\rho]\hat{\rho} - \hat{\rho}\hat{H}[\rho]S^{-1}\right) \quad (1)$$

where $\hat{\rho}$ is the single electron density matrix, S^{-1} is the inverse of the overlap matrix and $\hat{H}$ is the SCC-DFTB Hamiltonian.

The absorption spectra for all systems were obtained by applying a Dirac delta pulse type perturbation. When the electric field used is small, the system is within the linear response regime and the dipole moment is defined as:

$$\langle\mu(t)\rangle = \int_0^\infty \alpha(t-\tau)E(\tau)\mathrm{d}\tau \quad (2)$$

where $\alpha(t-\tau)$ is the polarizability along the axis over which the external field $E(t)$ is applied, or in the frequency domain:

$$\alpha(w) = \frac{\langle\mu(w)\rangle}{E(w)} \quad (3)$$

where the average of the imaginary part of the frequency-dependent dynamic polarizability around the three Cartesian axes is proportional to the absorption spectrum.

The study of the electronic dynamics of the systems was carried out by comparing results of the application of a sinusoidal perturbation adjusted with the frequency of maximum absorption of the spectrum with the application of a large series of sinusoidal perturbations to each system corresponding to the range of wavelengths of the solar spectrum at sea level (300–2500 nm). The excitations were carried out using an electric field of 1.35×10^9 W cm^{-2} with a direction consistent with the maximum dynamic polarizability direction for each wavelength. The purpose of these calculations is to show whether the results for the charge transfer process that are obtained when studying it at the maximum dye absorption are different to what is obtained from broadband illumination.

The method described in this section has already been used previously to calculate the absorption spectra of chlorophylls,[56,57] silver, aluminum[58,59] and TiO_2[60] nano-clusters, and graphene nano-flakes,[61] the dynamics of charge transfer in dye–semiconductor[49–51] and donor–acceptor molecular complexes,[62] the effect of intercalation compounds on the absorption spectra of DNA,[63] and the photoinduced dynamics in DNA-stabilized silver nanocluster emitters.[64] Other groups have used more exact quantum chemical methods, similar to TD-DFTB, such as the *ab initio* TD-DFT approach. For dye–quantum dot systems such as porphyrin–CdSe/ZnS, the method qualitatively explains the results observed experimentally.[65] TD-DFT has also been used for the rational design of new dyes, which may lead to more efficient cells.[66]

3 Results and discussion

For all calculations performed in this work, we used a 270 atom (90 TiO_2 units, see Fig. 2) anatase nanocluster, and CAT, ALZ and FSD101[20] as sensitizer dyes (Fig. 3). The TiO_2 nanocluster structures are the same as those that were described by some of us previously,[50] and they were generated from molecular dynamic simulations at 300 K.

The geometry optimization of the dyes and the dye–nanoparticle systems was performed using the dftb$^+$ package and was restricted, in the case of the complexes, to the dye coordinates and five TiO_2 units closest to the dye anchoring point.

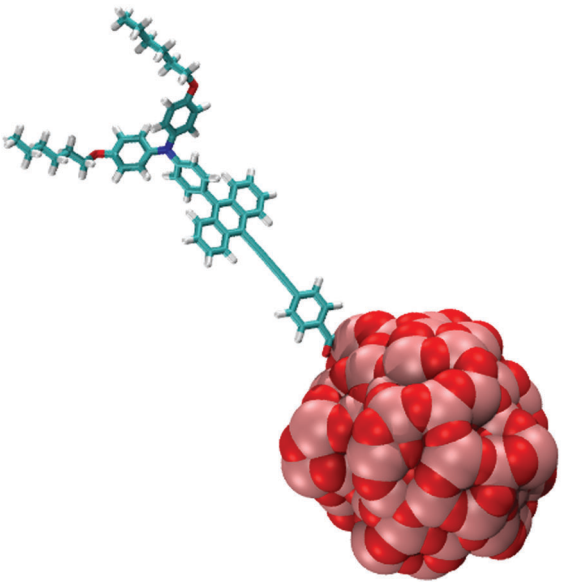

Fig. 2 Atomic structure of the FSD101–TiO_2 complex.

Table 1 compares the absorption energies obtained theoretically with TD-DFTB and experimentally from the literature, both for free dyes and for the dye–NP complexes. It is important to note that the absorption spectra of dyes and experimentally measured complexes were recorded in organic solvents whereas our results correspond to the system in a vacuum. The tabulated values correspond to the lowest excitation energy in each case.

Table 1 Lowest energy excitation absorption energy values (in eV) for free dyes and NP–dye systems obtained by the TD-DFTB method (in vacuum) and experimental values found in the literature

	Free exc./eV		Adsorbed exc./eV	
Dye	TD-DFTB	Exp. value	TD-DFTB	Exp. value
ALZ	2.85	2.88[67]	2.44	2.48[67]
CAT	4.55	4.43[68]	3.00	3.18[68]
FSD101	2.40	2.77[20]	2.43	2.89[20]

It is worth noting that, as discussed below, the appearance of a new absorption band when CAT is adsorbed on the NP agrees with what is observed experimentally. Both absolute values of the absorption energies agree qualitatively in general and even quantitatively in the case of ALZ. The change in energy upon absorption agrees as well with the exception of FSD101 for which the change (as noted below) is very small. Regarding the absorption ratios between the free dye and adsorbed dye bands, in general, they agree qualitatively with experimental data. In the case of ALZ, although both theoretically and experimentally, the absorption increases upon adsorption, in the experimental case, the increase is larger. From previous studies,[49,50] it is known that ALZ is a molecule that exhibits an indirect (type-I) mechanism of injection whereas CAT exhibits a direct mechanism (type-II) for electron injection. These works suggested that it is possible to predict the electronic injection mechanism of the complexes, analyzing and comparing the absorption spectra of the dye and the isolated NP with respect to the spectrum of the dye–TiO_2 system.

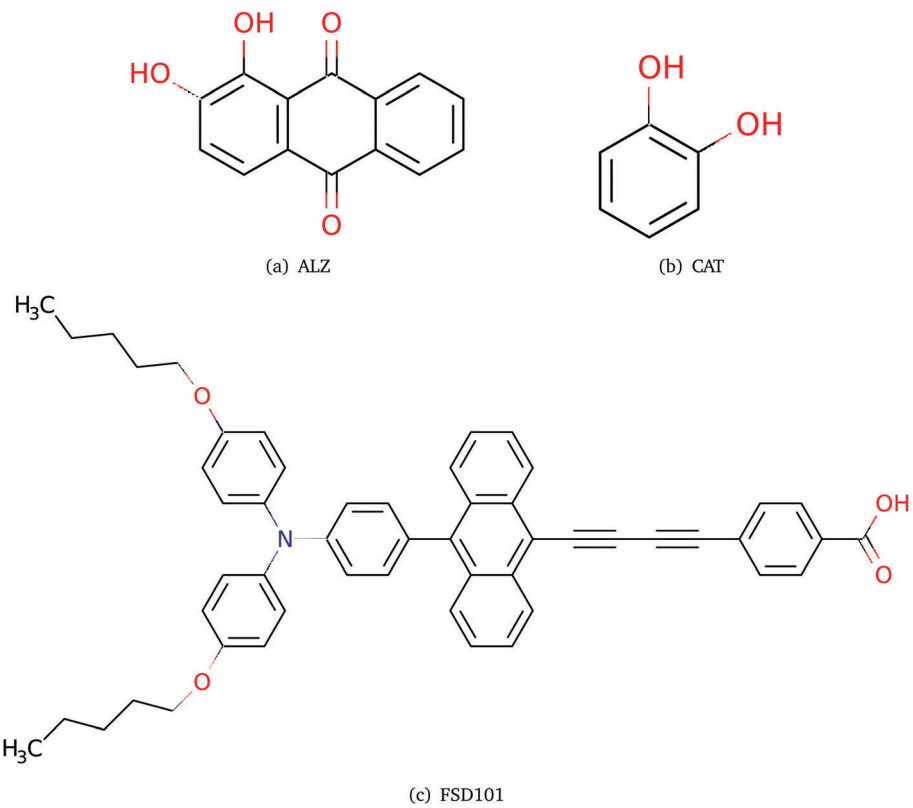

Fig. 3 Studied compounds.

In the spectrum of the ALZ–NP system, it can be observed that the lowest-energy band suffers a red shift upon adsorbing the dye onto the TiO_2 NP but no new absorption band appears in the visible region when this occurs. The CAT–NP system shows the appearance of a new transition band at 3.00 eV when adsorbed onto the NP. In the case of the FSD101 molecule, the spectrum shows no significant shift for the lowest-energy band nor the appearance of new bands when the dye is anchored to the semiconductor; the mechanism of electronic injection is therefore indirect.

Fig. 5 shows the evolution of the time-dependent charge distribution in the dye and the NP upon photo-excitation of dye–TiO_2 complex with a sinusoidal time-dependent electric field perturbation with the frequency of the lowest-energy absorption band of each spectrum: 2.44 eV for ALZ, 3.00 eV for CAT and 2.43 eV for FSD101, and the direction of the transition dipole moment of the total system. In general, in Fig. 5, it can be observed that there is a net transfer of charge in all the systems. CAT and FSD101 molecules become increasingly positively charged as time increases, whereas the cluster, in both systems, gets negatively charged. These results indicate that with the photo-excitacion of the dye at its maximum absorption, the charge is transferred from the dye to the conduction band of the NP, a process that corresponds to electron injection. Nevertheless, in the case of ALZ, when the time increases, the molecule becomes negatively charged whereas the semiconductor acquires a positive charge. The charge, in this system, is transferred from the valence band of the semiconductor to the HOMO of the dye, in contrast with the other studied dyes, indicating hole injection.

Fig. 6 shows the absorption spectra of the complexes, the average charge transfer current values over a simulation window of 100 fs and the quantum efficiency of the charge injection process. These last values were obtained by calculating the slope of the charge with respect to time for each of the energies analyzed in the simulation window, that is, tuning lasers with sinusoidal waves with wavelengths that are within the solar spectrum at sea level: (300–2500) nm or (0.5–4.15) eV. The absorbed energy (used as input for the quantum efficiency calculation) was calculated in the same manner, from the power calculated as the slope obtained from fitting the system total energy *versus* time within the simulation window. In all cases, within the simulation window, both the transferred charge and the total energy are linear over time, consistent with the fact that the simulations are carried out within the linear response regime.

The values of current obtained for CAT–TiO_2 are positive at all incident wavelengths and a maximum (positive) current is observed at 3.00 eV. This value coincides with the maximum absorption of the optical absorption spectrum. The fact that the maximum value of the current obtained as a function of the dye charges is positive and is observed as a consequence of illuminating the system with the wavelength of the maximum absorption indicates electron transfer, which coincides with what was previously observed by some of us.[50]

For the other two dyes, the positive and negative values of average current in graphs (a) and (c) indicate the existence of two different injection directions that operate at different wavelenths within the solar spectrum. For ALZ–TiO_2 (see graph (a)), from 1.8 eV to 3.32 eV, hole transfer is observed and from 3.32 eV to 4.15 eV, electron transfer is observed. In this case, a maximum current is also observed at the maximum absorption at 2.44 eV but the value is negative, which means that the molecule becomes negatively charged over time, corresponding to a hole transfer process.

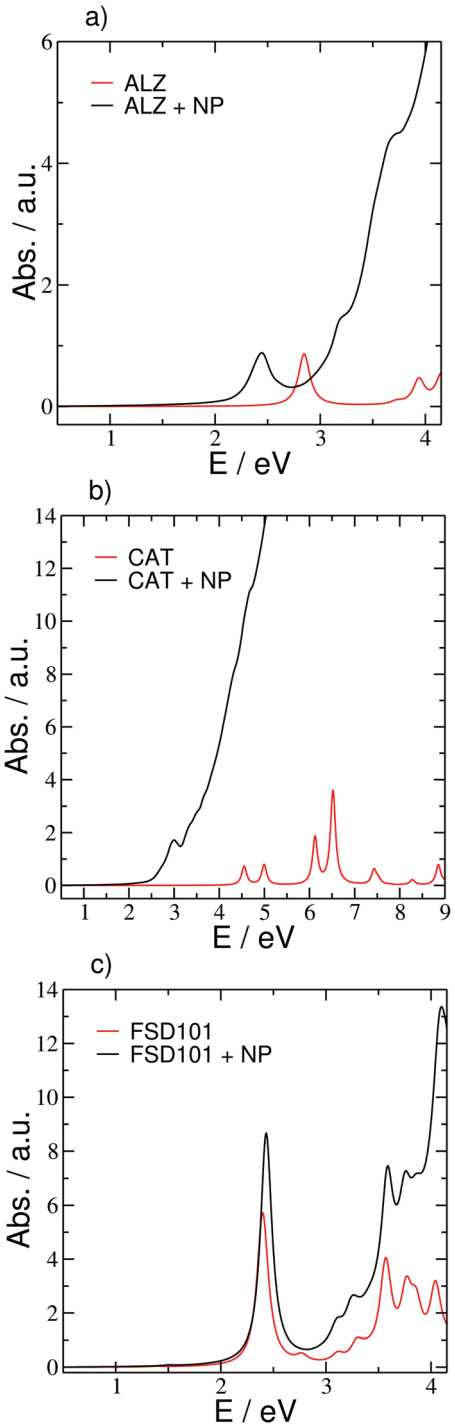

Fig. 4 Superposition of the optical spectra of the three dyes and dyes anchored to the TiO_2 NP. ALZ (a), CAT (b) and FSD101 (c).

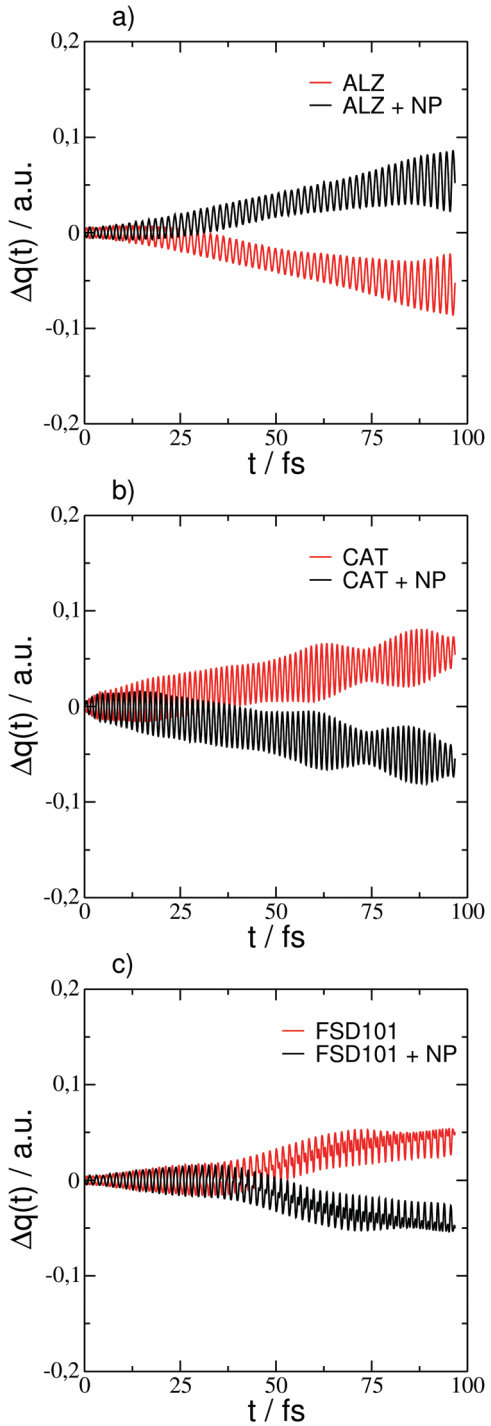

Fig. 5 Charge evolution during electron injection simulations for illumination at 2.44 eV of the TiO_2 + ALZ system (a), at 3.00 eV of the TiO_2 + CAT system (b) and at 2.43 eV of the TiO_2 + FSD101 system (c).

In the current graph (see graph c) of FSD101–TiO_2, it is hole transfer that is observed in the intervals (1.8–2.3) eV and (2.5–4.15) eV while electron transfer is observed in the interval (2.3–2.5) eV. The current is maximal when the system is illuminated with the wavelength of the absorption maximum at 2.43 eV and it shows electron transfer as in the case of CAT–TiO_2. In Fig. 6, it is also observed that when illuminated at higher energies or shorter wavelengths, which correspond to the absorption band of the NP (see the absorption spectra), for the ALZ–TiO_2 and FSD101–TiO_2 complexes, charge is transferred in the opposite direction than the one obtained when illuminated with an energy that the dye absorbs, and this behavior is not observed for CAT–TiO_2. Finally, it can also be seen from the figure that the average current graphs reveal more information about the absorption bands of the dye in the system, with respect to the absorption spectrum. Many features can be determined within the absorption range where the NP band dominates the spectrum.

It is a general feature of all the studied systems that hole transfer occurs only above a certain energy threshold. This can be rationalized in terms of the diagrams shown in Fig. 1. The lowest energy transitions are all of the kind depicted in the left panel of Fig. 1. With the exception of CAT, for which the lowest energy transition corresponds to the situation shown in the right panel of the same figure. As excitation energy increases, excitations promote electrons from orbitals below the HOMO, which must overlap more strongly with the valence band of the nanoparticle, thus showing hole transfer.

The quantum efficiency of the charge transfer process between dye and NP (γ) was calculated for each energy from the relation between the absorbed photon flux and the number of charge carriers collected. To obtain the number of photons per second, the absorbed power at each frequency was calculated as the slope of the energy as a function of time (as mentioned before), while the values of the number of charge carriers were obtained from the average currents obtained previously. The results of efficiency are shown in Fig. 6; for ALZ–TiO_2, a maximum peak is observed at 2.23 eV with $\gamma = -0.89$. As the value obtained is negative, in this system, the highest efficiency of the charge transfer process is observed when electrons from the valence band (VB) are injected into the dye.

For CAT, a peak with $\gamma = 1.7$ is observed at 3.00 eV and electrons are injected from the dye to the CB. In this case, unlike ALZ, the energy of the maximum absorption coincides with the energy of the highest value of γ. The fact that the efficiency has a value greater than 1 for this system can be attributed to the direct injection mechanism. As described by some of us before,[49] a first order perturbation theory approach in which the population injected into the LUMO escapes at a constant rate to the CB is appropriate. In this case, the energy input is used to pump electrons from the HOMO to the LUMO, which then escape to a manifold of CB states in an incoherent and adiabatic (with no energy investment) fashion characterized by a simple rate constant. In this manner, a large quantum efficiency can be obtained if the LUMO state population is maintained at a steady state, investing a small amount of energy to promote electrons that are then transferred adiabatically at no further energy cost.

For FSD101, a maximum efficiency of $\gamma = -0.18$ for an illumination of around 3.26 eV is observed, caused by hole transfer. It is observed, on the other hand, that at energies lower than 2.30 eV, a large efficiency is achieved in a zone of the spectrum for which no appreciable charge transfer nor energy absorption can be observed. A similar behavior is observed in

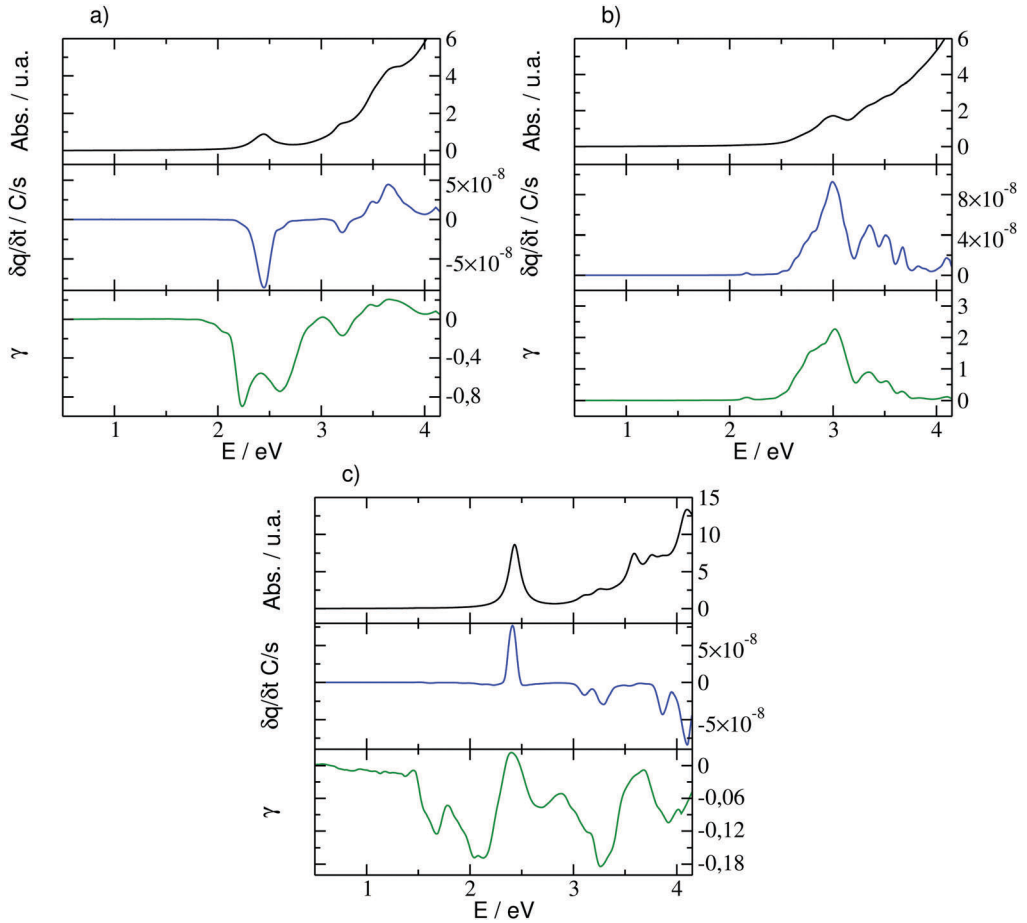

Fig. 6 Absorption spectra of the dye–TiO_2 systems compared with the slopes of the time-dependent averages of the charges over time and quantum efficiency of the transfer process between dye and NP (γ) for ALZ (a), CAT (b) and FSD101 (c) as a function of energy (E). Positive values in the slopes and quantum efficiencies correspond to electron transfer from the dye to the nanoparticle whereas negative values indicate hole transfer.

the case of ALZ, where the maximal efficiencies correspond to the sides of the main absorption band at 2.33 eV.

In the case of both these dyes, the coupling to the NP states is lower than that of CAT, as can be inferred from the absorption spectra shown in Fig. 4. The coupling of ALZ can be characterized as intermediate between CAT and FSD101, since there is a small spectral overlap between the absorption edge of the NP and the dye and a renormalization of the excitation of about 0.3 eV is observed. The coupling of FSD101 is the lowest of the three cases studied, as manifested by the very small energy renormalization and small spectral overlap.

In the cases where the coupling is small, one cannot assume that in the resonant regime, the LUMO population of the dye is in a steady state since the coupling is not strong enough to drive charge out of the LUMO at the same rate as it is pumped by the external field. It is therefore seen that in the resonant cases of both ALZ and FSD101, the quantum efficiency is not maximal. Higher quantum efficiencies are achieved in zones of the spectrum that show small absorption and in turn a non-negligible charge transfer. In these situations, since the rate of population of the LUMO is small, even a small coupling to the NP can drive away all of the pumped population and the system is in a regime similar to that described in the previous paragraph.

For the dye FSD101, in Fig. 6, it is observed that in the range between 0.5 and 2.0 eV, there is no appreciable absorption or current, at the scale shown. However, the overall charge transfer efficiency is appreciable. Using a time-dependent DFTB

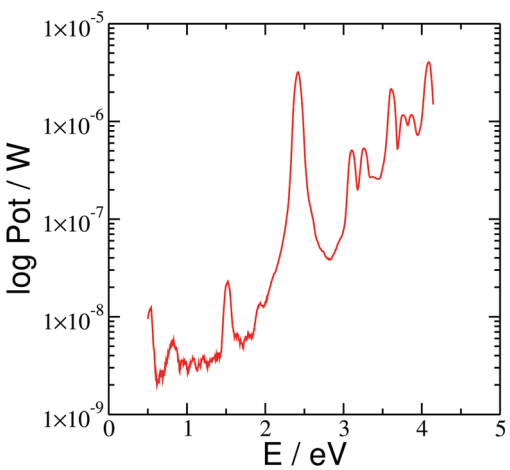

Fig. 7 Linear response spectrum for the FSD101–NP system: logarithm of the molar coefficient of extinction (ε) as a function of energy (E).

calculation based on a linear response theory as implemented in the dftb$^+$ package,[69] we observe (see Fig. 7) absorption starting at 1.5 eV and throughout the analyzed range that is not appreciable in the other graphs but that is present and influences the efficiency.

4 Conclusions

The spectra, in addition to showing a good concordance with the experimental data, reveal the mechanisms of electronic injection of each of the systems: CAT–TiO_2 presents a type II (or direct) mechanism while ALZ–TiO_2 and FSD101–TiO_2 present a type I (or indirect) mechanism.

Illuminating with the energy of the maximum of absorption, we observed charge transfer in the three complexes. In CAT–TiO_2 and FSD101–TiO_2, electronic injection occurs from the dye to the NP, whereas in ALZ–TiO_2, the charge transfer occurs from the NP to the dye.

The main conclusions of this work are related to the results obtained from the study of the system under illumination over a broad band of energies, corresponding to the whole breadth of the solar spectrum.

In this case, we observe that for CAT, there is only electron transfer while for the other complexes, depending on the incident energy, there can be a transfer of holes or electrons.

Finally, upon analysis of the efficiencies, it was observed that the largest efficiency of the primary process of charge transfer does not necessarily occur when illuminating at the absorption maximum.

Furthermore, the overall efficiency is given by a compromise between hole and electron transfer. For ALZ–TiO_2 and FSD101–TiO_2, the highest efficiency occurs due to hole transfer and not with the energy of the maximum absorption. For CAT–TiO_2, the highest efficiency is caused by electron transfer with the energy of the absorption maximum.

Conflicts of interest

There are no conflicts to declare.

References

1 B. O'Regan and M. Gratzel, *Nature*, 1991, **353**, 737–740.
2 H. Zheng, Y. Tachibana and K. Kalantar-Zadeh, *Langmuir*, 2010, **26**, 19148–19152.
3 X. Chen and S. S. Mao, *Chem. Rev.*, 2007, **107**, 2891–2959.
4 M. D. McGehee, *Science*, 2011, **334**, 607–608.
5 O. V. Prezhdo, W. R. Duncan and V. V. Prezhdo, *Prog. Surf. Sci.*, 2009, **84**, 30–68.
6 F. Odobel, L. L. Pleux, Y. Pellegrin and E. Blart, *Acc. Chem. Res.*, 2010, **43**, 1063–1071.
7 F. Odobel, Y. Pellegrina, E. A. Gibsonb, A. Hagfeldtc, A. L. Smeighd and L. Hammarströmd, *Coord. Chem. Rev.*, 2012, **256**, 2414–2423.
8 M. Buchalska, J. Kuncewicz, E. Świętek, P. Łaabuz, T. Baran, G. Stochel and W. Macyk, *Coord. Chem. Rev.*, 2013, **257**, 767–775.
9 A. Hagfeldt, G. Boschloo, L. Sun, L. Kloo and H. Pettersson, *Chem. Rev.*, 2010, **110**, 6595–6663.
10 D. Dini, *Phys. Chem. Commun.*, 2016, **3**, 14–51.
11 I. Hod, Z. Tachan, M. Shalom and A. Zaban, *Phys. Chem. Chem. Phys.*, 2013, **15**, 6339.
12 D. Xiong, H. Wang, W. Zhang, X. Zeng, H. Chang, X. Zhao, W. Chen and Y. bing Cheng, *J. Alloys Compd.*, 2015, **642**, 104–110.
13 O. Langmar, C. R. Ganivet, A. Lennert, R. D. Costa, G. D. L. Torre, T. Torres and D. M. Guldi, *Angew. Chem., Int. Ed.*, 2015, **54**, 7688–7692.
14 T. Jiang, M. Bujoli-Doeuff, Y. Farre, Y. Pellegrin, E. Gautron, M. Boujtita, L. Cario, S. Jobic and F. Odobel, *RSC Adv.*, 2016, **6**, 112765.
15 T. Iwamoto, Y. Ogawa, L. Sun, M. S. White, E. D. Glowacki, M. C. Scharber, N. S. Sariciftci, K. Manseki, T. Sugiura and T. Yoshida, *J. Phys. Chem. C*, 2014, **118**, 16581–16590.
16 K. J. Chen, A. D. Laurent, F. Boucher, F. Odobel and D. Jacquemin, *J. Mater. Chem. A*, 2016, **4**, 2217–2227.
17 S. Du, P. Cheng, P. Sun, B. Wang, Y. Cai, F. Liu, J. Zheng and G. Lu, *Chem. Res. Chin. Univ.*, 2014, **30**, 661–665.
18 M. Miclau, N. Miclau, R. Banica and D. Ursu, *Mater. Today*, 2017, **4**, 6975–6981.
19 J. Sarkar and S. Bhattacharyya, *Arch. Thermodyn.*, 2012, **33**, 23–40.
20 J. K. Fang, T. Sun, Y. Tian, Y. Zhang, C. Jin, Z. Xu, Y. Fang, X. Hu and H. Wang, *Mater. Chem. Phys.*, 2017, **195**, 1–9.
21 C. Jia, Z. Wan, J. Zhang, Z. Li, X. Yao and Y. Shi, *Spectrochim. Acta, Part A*, 2012, **86**, 387–391.
22 M. Li, L. Kou, L. Diao, Q. Zhang, Z. Li, Q. Wu, W. Lu, D. Pan and Z. Wei, *J. Phys. Chem. C*, 2015, **119**, 9782–9790.
23 A. Mahmood, S. U.-D. Khan and U. A. Rana, *J. Comput. Electron.*, 2014, **13**, 1033–1041.
24 W. Zhang, Y. Wu, H. Zhu, Q. Chai, J. Liu, H. Li, X. Song and W. H. Zhu, *ACS Appl. Mater. Interfaces*, 2015, **7**, 26802–26810.
25 J. Wang, K. Liu and X. Zhan, *Chem. Rev.*, 2016, **116**, 14675–14725.
26 A. S. Beni, M. Zarandi, A. R. Madram, Y. Bayat and R. Ghahary, *Electrochim. Acta*, 2015, **186**, 504–511.
27 M. Godfroy, C. Aumaitre, F. Caffy, Y. Kervella, L. Cabau, L. Pellejà, P. Maldivi, S. Narbey, F. Oswald, E. Palomares, D. Joly and R. Demadrille, *Dyes Pigm.*, 2017, **146**, 352–360.
28 S. Namuangruk, S. Jungsuttiwong, N. Kungwan, V. Promarak, T. Sudyoadsuk, B. Jansang and M. Ehara, *Theor. Chem. Acc.*, 2016, **135**, 1–13.
29 H. Feng, R. Li, Y. Song, X. Li and B. Liu, *J. Power Sources*, 2017, **345**, 59–66.
30 L. Han, J. He and S. Jiang, *Res. Chem. Intermed.*, 2017, **43**, 5779–5794.
31 o. Birel, S. Nadeem and H. Duman, *J. Fluoresc.*, 2017, **27**, 1075–1085.
32 S. Mathew, A. Yella, P. Gao, R. Humphry-Baker, B. F. E. Curchod, N. Ashari-Astani, I. Tavernelli, U. Rothlisberger,

M. K. Nazeeruddin and M. Grätzel, *Nat. Chem.*, 2014, **6**, 242–247.
33 A. Yella, H.-W. Lee, H. N. Tsao, C. Yi, A. K. Chandiran, M. K. Nazeeruddin, E. W.-G. Diau, C.-Y. Yeh, S. M. Zakeeruddin and M. Gratzel, *Science*, 2011, **334**, 629–634.
34 M. Mao, X. Zhang, B. Zhu, J. Wang, G. Wu, Y. Yin and Q. Song, *Dyes Pigm.*, 2016, **124**, 72–81.
35 U. Daniel, D. Anamaria, I. Sebarchievicia and M. Miclau, *Energy Procedia*, 2017, **112**, 497–503.
36 A. Morandeira, G. Boschloo, A. Hagfeldt and L. Hammarstro, *J. Phys. Chem. C*, 2008, 9530–9537.
37 Y. Mizoguchi and S. Fujihara, *Electrochem. Solid-State Lett.*, 2008, **11**, K78.
38 A. Morandeira, G. Boschloo, A. Hagfeldt and L. Hammarström, *J. Phys. Chem. B*, 2005, **109**, 19403–19410.
39 P. K. B. Palomaki, M. R. Civic and P. H. Dinolfo, *ACS Appl. Mater. Interfaces*, 2013, **5**, 7604–7612.
40 M. Borgström, E. Blart, G. Boschloo, E. Mukhtar, A. Hagfeldt, L. Hammarström and F. Odobel, *J. Phys. Chem. B*, 2005, **109**, 22928–22934.
41 M. Wild, J. Griebel, A. Hajduk, D. Friedrich, A. Stark, B. Abel and K. R. Siefermann, *Sci. Rep.*, 2016, 1–8.
42 S. Feihl, R. D. Costa, S. Pflock, C. Schmidt, J. Schönamsgruber, S. Backes, A. Hirsch and D. M. Guldi, *RSC Adv.*, 2012, **2**, 11495.
43 C. H. Chang, Y. C. Chen, C. Y. Hsu, H. H. Chou and J. T. Lin, *Org. Lett.*, 2012, **14**, 4726–4729.
44 D. Ameline, S. Diring, Y. Farre, Y. Pellegrin, G. Naponiello, E. Blart, B. Charrier, D. Dini, D. Jacquemin and F. Odobel, *RSC Adv.*, 2015, **5**, 85530–85539.
45 J. Warnan, J. Gardner, L. Le Pleux, J. Petersson, Y. Pellegrin, E. Blart, L. Hammarström and F. Odobel, *J. Phys. Chem. C*, 2014, **118**, 103–113.
46 Y.-S. Yen, W.-T. Chen, C.-Y. Hsu, H.-H. Chou, J. T. Lin and M.-C. P. Yeh, *Org. Lett.*, 2011, **13**, 4930–4933.
47 P. Naik, A. Planchat, Y. Pellegrin, F. Odobel and A. V. Adhikari, *Sol. Energy*, 2017, **157**, 1064–1073.
48 J. Y. Park, B. Y. Jang, C. H. Lee, H. J. Yun and J. H. Kim, *RSC Adv.*, 2014, **4**, 61248–61255.
49 M. B. Oviedo, X. Zarate, C. F. A. Negre, E. Schott, R. Arratia-Pérez and C. G. Sánchez, *J. Phys. Chem. Lett.*, 2012, **3**, 2548–2555.
50 C. F. A. Negre, V. Fuertes, M. B. Oviedo, F. Y. Oliva and C. G. Sánchez, *J. Phys. Chem. C*, 2012, **116**, 14748–14753.
51 C. F. a. Negre, K. J. Young, M. B. Oviedo, L. J. Allen, C. G. Sánchez, K. N. Jarzembska, J. B. Benedict, R. H. Crabtree, P. Coppens, G. W. Brudvig and V. S. Batista, *J. Am. Chem. Soc.*, 2014, **136**, 16420–16429.
52 Z. Yao, H. Wu, Y. Li, J. Wang, J. Zhang, M. Zhang, Y. Guo and P. Wang, *Energy Environ. Sci.*, 2015, 11–16.
53 M. Elstner, D. Porezag, G. Jungnickel, J. Elsner, M. Haugk, T. Frauenheim, S. Suhai and G. Seifert, *Phys. Rev. B: Condens. Matter Mater. Phys.*, 1998, **58**, 7260–7268.
54 B. Aradi, B. Hourahine and T. Frauenheim, *J. Phys. Chem. A*, 2007, **111**, 5678–5684.
55 G. Dolgonos, B. Aradi, N. H. Moreira and T. Frauenheim, *J. Chem. Theory Comput.*, 2010, **6**, 266–278.
56 M. B. Oviedo, C. F. A. Negre and C. G. Sánchez, *Phys. Chem. Chem. Phys.*, 2010, **12**, 6706.
57 M. B. Oviedo and C. G. Sánchez, *J. Phys. Chem. A*, 2011, **115**, 12280–12285.
58 O. A. Douglas-Gallardo, M. Berdakin and C. G. Sánchez, *J. Phys. Chem. C*, 2016, **120**, 24389–24399.
59 O. A. Douglas-Gallardo, G. J. Soldano, M. M. Mariscal and C. G. Sanchez, *Nanoscale*, 2017, **9**, 17471–17480.
60 V. C. Fuertes, C. F. a. Negre, M. B. Oviedo, F. P. Bonafé, F. Y. Oliva and C. G. Sánchez, *J. Phys.: Condens. Matter*, 2013, **25**, 115304.
61 C. M. Wettstein, F. P. Bonafé and M. B. Oviedo, *J. Chem. Phys.*, 2016, 224305.
62 C. R. Medrano, M. B. Oviedo and C. G. Sánchez, *Phys. Chem. Chem. Phys.*, 2016, **18**, 14840–14849.
63 E. N. Primo, M. B. Oviedo, C. G. Sánchez, M. D. Rubianes and G. A. Rivas, *Bioelectrochemistry*, 2014, **99**, 8–16.
64 M. Berdakin, M. Taccone, K. J. Julian, G. Pino and C. G. Sánchez, *J. Phys. Chem. C*, 2016, **120**, 24409–24416.
65 E. Zenkevich, A. Stupak, C. Goehler, C. Krasselt and C. von Borczyskowski, *ACS Nano*, 2015, **9**, 2886–2903.
66 S. Ramkumar and P. Manidurai, *Spectrochim. Acta, Part A*, 2017, **173**, 425–431.
67 R. Huber, S. Spörlein, J. E. Moser, M. Grätzel and J. Wachtveitl, *J. Phys. Chem. B*, 2000, **104**, 8995–9003.
68 Y. Wang, K. Hang, N. A. Anderson and L. Tianquan, *J. Phys. Chem. B*, 2003, **107**, 9434–9440.
69 T. A. Niehaus, S. Suhai, F. Della Sala, M. Elstner, G. Seifert and T. Frauenheim, *Phys. Rev. B: Condens. Matter Mater. Phys.*, 2001, **63**, 1–9.